Density invariant vibrational modes in disordered colloidal crystals

N. L. Green, D. Kaya, C. E. Maloney, and M. F. Islam

Density Invariant Vibrational Modes in Disordered Colloidal Crystals

N. L. Green[1], D. Kaya[2], C. E. Maloney[3], and M. F. Islam[2,*]

[1]*Department of Chemical Engineering,* [2]*Department of Materials Science and Engineering,*
and [3]*Department of Civil and Environmental Engineering*
Carnegie Mellon University, Pittsburgh, Pennsylvania 15213-3890 and
[*]*email: mohammad@cmu.edu*

We experimentally measure the density of states (DOS) and dynamical structure factor (DSF) arising from the thermal fluctuations in a colloidal crystal composed of thermally sensitive micron-sized hydrogel particles at several different particle volume fractions, ϕ. Particle positions are tracked over long times using optical microscopy and particle tracking algorithms in a single two dimensional (2D) [111] plane of a 3D face-centered-cubic single crystal. The dynamical fluctuations are spatially heterogeneous while the lattice itself is highly ordered. At all ϕ, the DOS exhibits an excess of low frequency modes, a so-called boson peak (BP), and the DSF exhibits a cross-over from propagating to non-propagating behavior, a so-called Ioffe-Regel (IR) crossover, at a frequency somewhat below the BP for both longitudinal and transverse modes. As we tune ϕ from 0.64 to 0.56, the Lindemann parameter grows from $\sim 3\%$ to $\sim 8\%$; however, the shape of the DOS and DSF remain largely unchanged when rescaled by the Debye level. This invariance indicates that the effective degree of disorder remains essentially constant even in the vicinity of melting.

I. INTRODUCTION

Over the last two decades, there has been much work examining vibrational properties in disordered solids; primarily in structural glasses. One important question is whether the effective disorder in the medium changes under changes in external parameters such as pressure [1], temperature [2], or density [3, 4]. Most studies have focused on the density of states (DOS) to provide some measure of these changes. In some glasses [3], the DOS is invariant under changes in density after a rescaling of energy by the Debye energy level, as long the geometry of the glass does not change, signaling an invariance in the underlying effective disorder. In others, when pressure [1], temperature [2], or density [4] is changed, the DOS is *not* invariant. It is not clear *a priori* which systems will exhibit this simple scaling property and which will exhibit more complex changes in the underlying disorder.

Colloidal systems have been studied intensely over the last decade as analogs for atomic systems [4–11], primarily because colloidal particles offer a distinct advantage over atoms in that colloids can be tracked directly using optical microscopy. Most studies have used glass or polymer particles which behave as perfectly rigid spheres [5–7, 9]. More recently, however, various groups have begun to study particles which are soft enough such that they can deform appreciably under Brownian forces [4, 8, 10, 11].

We have previously shown that crystals built out of such soft particles can display dynamics which are spatially heterogeneous despite a very high degree of crystalline order [11]. These systems represent a new class of disordered solid in which the underlying disorder does not arise from geometry but instead arises from disorder in the interactions between the particles. Similar disorder is present in models of elastically disordered lattices [12, 13]. Previously, we showed that the DOS of these disordered crystals exhibits an excess of modes, a so-called boson peak (BP) [11], at low frequency, as seen in structural glasses.

Here, we show that the dynamical structure factor (DSF), for both the transverse and longitudinal modes, and DOS remain essentially constant with particle volume fraction, ϕ, after Debye rescaling, even close to the melting transition where the Lindemann parameter reaches over 8%. The DSF contains information about the *spatial structure* of the vibrational modes which is absent in the DOS and provides a much stronger test of Debye scaling. The disordered crystal we study is a three dimensional (3D) face-centered-cubic (fcc) lattice built by deposition of micron-sized hydrogel particles, resulting in a lattice with vertical [111] axis. We monitor particle positions in a single horizontal 2D [111] plane of the 3D crystal via optical microscopy and record the two-point correlations in the displacement field obtained by averaging over many statistically independent observations [4, 11, 14]. Assuming that the *dynamics* of the particles are governed by the same harmonic energy function that governs the displacement probabilities allows one to express the DOS and DSF in terms of the two-point correlations. The DOS and DSF then represent our primary window on the effective disorder in the interactions between the particles and its ϕ dependence.

II. EXPERIMENTAL

Our temperature sensitive microgel particles were synthesized via dispersion polymerization of *N*-isopropylacrylamide (NIPAm) and acrylic acid (AA) [11]. The microgel particles were then suspended in 20 mM

Tris base buffer at pH = 8. In this buffer, the particles can be considered sterically stabilized; the measured pair interaction potential between the particles in dilute suspension [15] did not show any long range electrostatic interactions due to AA groups [11]. The size polydispersity of the microgel particles, measured using dynamic light scattering (DLS), was < 4%. Fig. 1 shows that the hydrodynamic diameter, measured by DLS, changed linearly with temperature over a temperature range of 20°C to 30°C.
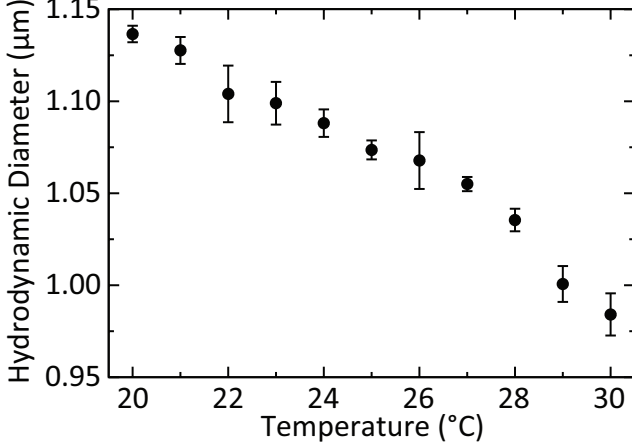

FIG. 1: The temperature dependence of the hydrodynamic diameter as obtained using dynamic light scattering.

We created face-centered-cubic (fcc) crystals at the highest volume fraction using the microgel colloids within a glass sample chamber of dimensions $18 \times 6 \times 0.1$ mm, with the [111] plane parallel to the glass surface. The grains within the fcc crystal had dimensions of a few millimeters parallel to the glass surface and $\sim 60 \mu m$ perpendicular to the glass surface. Since the microgel particles were more than 95% water, they were almost index and density matched. We collected $21,000$ bright-field images at a rate of 30 frames per second of a single slice of a [111] plane that was $30 - 40 \mu m$ away from both glass surfaces and near the center of a grain using an optical microscope (Leica DMI 6000B) equipped with a CCD camera, $100\times$ oil objective (N.A. 1.4) and oil condenser (N.A. 1.25). The temperature of the sample was maintained using stage (WP-16; Warner Instruments) and objective warmers (Warner Instruments) to 0.1°C. At fixed particle number density, the temperature is increased in steps. Since the hydrodynamic radius decreases with temperature, this results in a decrease in the nominal volume fraction. After each temperature decrease, we waited 6-8 hours for the sample temperature to equilibrate. The ϕ is scanned from 0.64 down to 0.56 in steps of 0.2 by increasing temperature from 21.4°C to 25.0°C. At each ϕ, we tracked the positions of $2,300$ particles using standard particle tracking algorithms [16, 17].

At each temperature, we make many statistically independent observations of the particle displacements, $u_{i\alpha}$, away from their time averaged position to ensure that

the two-point correlation matrix, $G_{i\alpha j\beta} = \langle u_{i\alpha} u_{j\beta} \rangle$ is well converged [11]. Here Latin indices indicate particle identity and Greek indicate Cartesian components. As expected, $G_{i\alpha j\beta}$ increases with decreasing ϕ as the system nears the melting transition. As pointed out earlier [11], $\langle u_{i\alpha} u_{i\alpha} \rangle$ varies from particle-to-particle in these disordered crystals. The RMS particle-to-particle fluctuation in $\langle u_{i\alpha} u_{i\alpha} \rangle$ is between 0.06 and 0.08 times the average $\langle u_{i\alpha} u_{i\alpha} \rangle$, showing little dependence on ϕ. The average mean squared displacement showed a clear plateau at long time scales indicating solid-like behavior. Fig. 2 shows the average mean square displacements at three different ϕ.
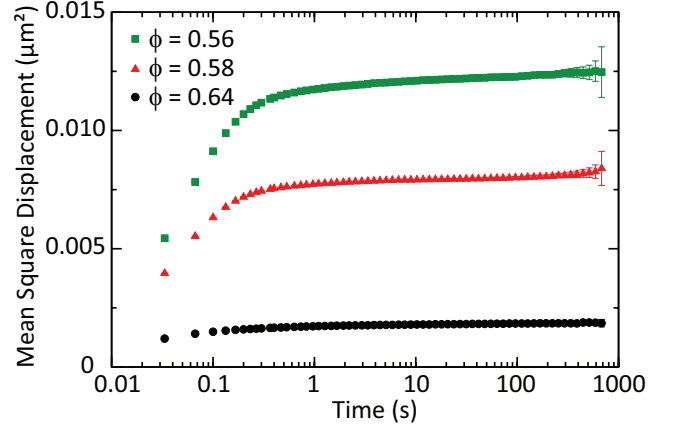

FIG. 2: (Color online) Mean square displacements for $\phi = 0.56(\square)$, $\phi = 0.58(\triangle)$ and $\phi = 0.64(\circ)$.

Within the harmonic approximation, in thermal equilibrium, $G_{i\alpha j\beta} = \langle u_{i\alpha} u_{j\beta} \rangle = \sum_p \frac{k_B T}{\lambda_p} \psi_{i\alpha}^p \psi_{j\beta}^p$, where k_B is Boltzmann's constant, T is the temperature, and $\psi_{i\alpha}^p$ is the p-th energy eigenmode with eigenvalue λ_p. We diagonalize $G_{i\alpha j\beta}$ using the eig() routine in MATLAB to find the full eigenmode spectrum. If one assumes that the dynamics are Hamiltonian, then $m\ddot{u}_{i\alpha} = \sum_{j\beta p} \lambda_p \psi_{i\alpha}^p \psi_{j\beta}^p u_{j\beta}$ and the energy eigenvalues may be converted to vibrational frequencies [4]: $m\omega_p^2 = \lambda_p$ where m is the particle mass.

III. RESULTS AND DISCUSSION

The DOS, $dN/d\omega = g_\omega$, where N is the mode index, is shown in Fig. 3 for several ϕ. At low ω, $g_\omega \sim \omega^2$, so we normalize g_ω by ω^2. As previously shown [11], g_ω/ω^2 has a plateau at low ω followed by a BP, and finally a rapid decay. As with $\langle u^2 \rangle$, the location of the BP, ω_{BP}, varies with ϕ. However, when we scale ω by $\omega^* = \sqrt{\frac{k_B T}{m \langle u^2 \rangle}}$, the DOS plots reasonably collapse. We also observe that the height of the plateau in g_ω/ω^2 scales with ω^*, and we identify ω^* with the Debye frequency. The scaled location of BP, ω_{BP}/ω^* shows some very slight density dependence, moving to lower values at lower ϕ. It also

becomes slightly broader with a shorter plateau region at lower ϕ indicating a slight increase in the degree of effective disorder. However, the good collapse, in spite of these small changes, indicates that the primary effect of changes in ϕ is simply to reset the overall characteristic energy scale.
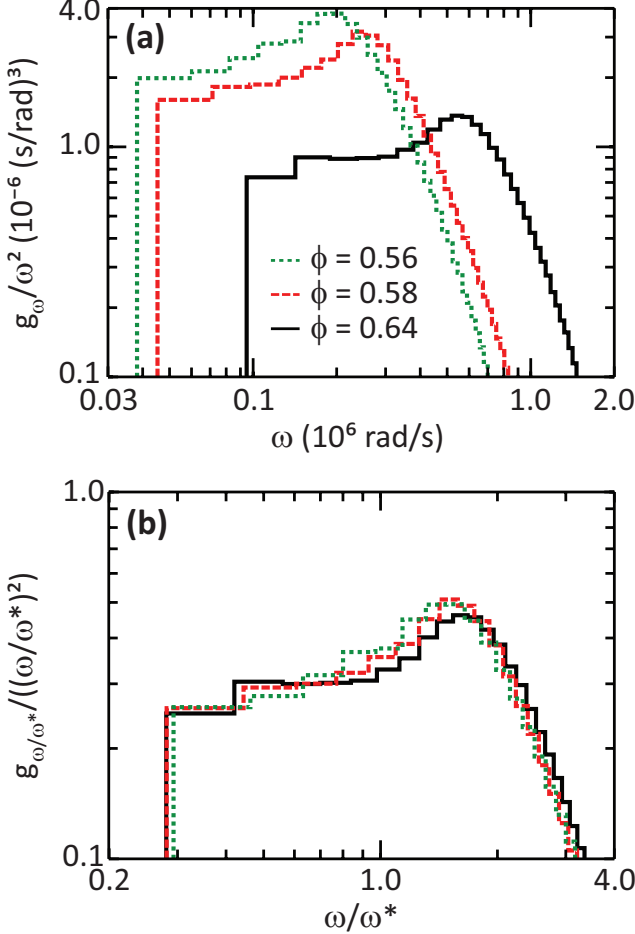

FIG. 3: (Color online) (a) The density of states (DOS) $g_\omega = dN/d\omega$ normalized by the frequency ω^2 for $\phi = 0.56, 0.58$, and 0.64. (b) Same as (a), but scaled by ω^* (see text). The approximate collapse of the DOS curves demonstrates that the main effect of changing ϕ is to rescale ω.

Next we focus on the planewave decomposition of the eigenmodes and its relationship to the DSF which would be observed in inelastic scattering experiments. The DSF can be written as [18–20]:

$$S_{\alpha\beta}(\vec{q}, \omega) = \frac{k_B T}{m\omega^2} q^2 \sum_p E_{\alpha\beta}^p(\vec{q}, \omega) \qquad (1)$$

where $E_{\alpha\beta}^p(\vec{q}, \omega)$ represents the projection of the p-th eigenmode, $\psi_{i\alpha}^p$, onto planewaves, $e^{i\vec{q}\cdot\vec{r}}$:

$$E_{\alpha\beta}^p(\vec{q}, \omega) = \sum_{ab} \psi_{\alpha pa}^* \psi_{\beta pb} e^{i\vec{q}\cdot\vec{r}_{ba}} \delta(\omega - \omega_p). \qquad (2)$$

We define $E_{\alpha\beta}(\vec{q}, \omega) = \sum_p E_{\alpha\beta}^p(\vec{q}, \omega)$ so that $S_{\alpha\beta}(\vec{q}, \omega) = \frac{k_B T}{m\omega^2} q^2 E_{\alpha\beta}(\vec{q}, \omega)$. $S(\vec{q}, \omega)$ encodes the contributions from various planewaves to the true eigenmodes at a given ω. As usual, one can decompose E (and S) into longitudinal ($E_L = E_{\alpha\beta} q_\alpha q_\beta / q^2$) and transverse ($E_T = \sum_\alpha E_{\alpha\alpha} - E_L$) components. We note that inelastic scattering experiments which probe density fluctuations are generally insensitive to S_T, while our microscopy/tracking techniques give us full access to both S_L and S_T.

Following reference [11], we interpolate each eigenmode onto a regular grid and perform an FFT to obtain $E_L^p(\vec{q})$ and $E_T^p(\vec{q})$. To regularize Eq. 2, we replace the delta function with a window with a 10% width in ω. Our results are not sensitive to the particular choice of window size. We then perform an isotropic average of $E(\vec{q}, \omega)$ over angles to obtain $E(q, \omega)$, again using a 10% window in $|\vec{q}|$ for averaging. We checked that restricting $\vec{q}$ to high symmetry directions (e.g., nearest neighbor and next nearest neighbor) gives similar results for $E(q, \omega)$.

In Fig. 4(a) (and 4(b)), we show $E_T(q, \omega)$ (and $E_L(q, \omega)$) for several different q at $\phi = 0.64$. For low enough q, both the transverse and longitudinal profiles have a single, well defined peak. The peak region can be well fit by the response function for a damped harmonic oscillator [21]:

$$E(q, \omega) \propto \frac{\Omega(q)^2 \Gamma(q)}{(\omega^2 - \Omega(q)^2)^2 + \omega^2 \Gamma(q)^2} \qquad (3)$$

with characteristic frequency, $\Omega(q)$, and damping rate $\Gamma(q)$. Ω and Γ both increase with q. Note that one generally obtains similar Ω and Γ from $E(q, \omega)$ and $S(q, \omega)$, although, as they differ by a factor of ω^2/q^2, the precise numerical values of Γ may be affected for very broad peaks [19]. Similar profiles are observed in scattering experiments [22, 23], and simulations [18, 19, 24–27].

In Fig. 4(c), we plot the fit parameters, $\Omega(q)$ and $\pi\Gamma(q)$, for both E_T and E_L. The solid line represents $q^{2/3}$ and is a good fit through the data for $\Omega(q)$. The $\Omega(q)$ profile is typically linear in scattering experiments and both 2D and 3D computer simulations as long as q is well below the (pseudo-) brillouin zone boundary. Departures from linearity in those cases represent true variations in elastic wave-speed and have important consequences for the DOS [27]. The large non-linearity observed here is rather benign and results from the fact that we make observations of a 2D slice of a 3D system. We have observed similar non-linearities when observing 2D slices in 3D computer simulations of perfect crystals. As we have argued elsewhere [11], to the extent that q represents a good quantum number, one expects $\omega \sim q^{2/3}$ at low ω. We also note that we currently do not know the q-dependence of $\Gamma(q)$ when observing 2D slices of 3D crystals.

When $\pi\Gamma \sim \Omega$, the peak width is on the order of the center frequency and the oscillator would become overdamped. Following conventional approaches [18, 27–29], we take the q at which $\Omega = \pi\Gamma$ to define the Ioffe-Regel
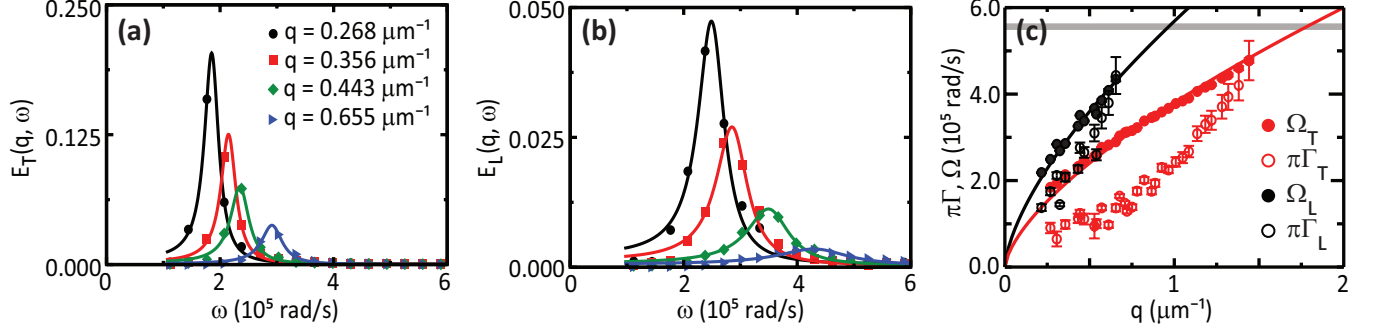
FIG. 4: (Color online) (a) Transverse planewave decomposition of eigenmodes, E_T, as a function of mode frequency, ω at several different wavevectors: $q = 0.268(\circ), 0.356(\square), 0.443(\diamond)$, and $0.655(\triangleright)$. (b) same as (a) but for longitudinal modes, E_L. The profiles can be well fit to the response function for a damped harmonic oscillator for the small q shown here. (c) Parameters, Ω and $\pi\Gamma$, of the fits to Eq. 3 as a function of q for the same data set as in (a) and (b). Solid line represents $q^{2/3}$. The horizontal gray line is ω_{BP}.

(IR) crossover. However, at the crossover, the damped oscillator fit to the $E(q,\omega)$ profile is not particularly robust, so $\Omega = \pi\Gamma$ should be taken as suggestive rather than definitive evidence that the given wavevector is sufficiently coupled to others so as to be overdamped. For the present system at $\phi = 0.64$, we see that the IR crossover is slightly below the BP for both longitudinal and transverse waves, with longitudinal waves crossing over at $\omega = 4.3 \times 10^5$ rad/s and transverse wave crossing at $\omega = 4.8 \times 10^5$ rad/s.

Many scattering experiments on atomic and molecular glasses show that longitudinal modes propagate at frequencies well above the BP. In *simulations* of structural glasses [18, 27], one observes that the IR limit occurs for the transverse modes near the BP, while the longitudinal modes propagate up to frequencies much higher than the BP. This is in sharp contrast to the behavior observed here in our system. These results suggest that the IR crossover for different branches of the DSF and its relationship to the BP may depend on the details of the underlying disorder.

In Fig. 5, we show both longitudinal and transverse branches for $\phi = 0.64$ along with $\phi = 0.56$. We scale Ω and $\pi\Gamma$ by ω_{BP} and we scale q by q^* where $\Omega(q^*) = \omega_{BP}$. The transverse branch in the $\phi = 0.56$ case crosses over much closer to ω_{BP}, but still somewhat below. As with $\phi = 0.56$, the longitudinal crossover is somewhat lower. At all ϕ, we find that the IR crossover for the transverse branch is below but within about 80% of the BP with the longitudinal IR crossover even further below.

The Debye scaling we observe here provides a strong check on the invariance of the underlying disorder with respect to changes in ϕ. The invariance of the DSF provides an even stronger check than the invariance of the DOS and indicates that the structure of the underlying normal modes is essentially unchanged, even in the vicinity of the melting transition. One might have imagined that on approach to melting, the particle dynamics would have become more hard-sphere-like, masking the effect of disorder coming from particle-to-particle varia-
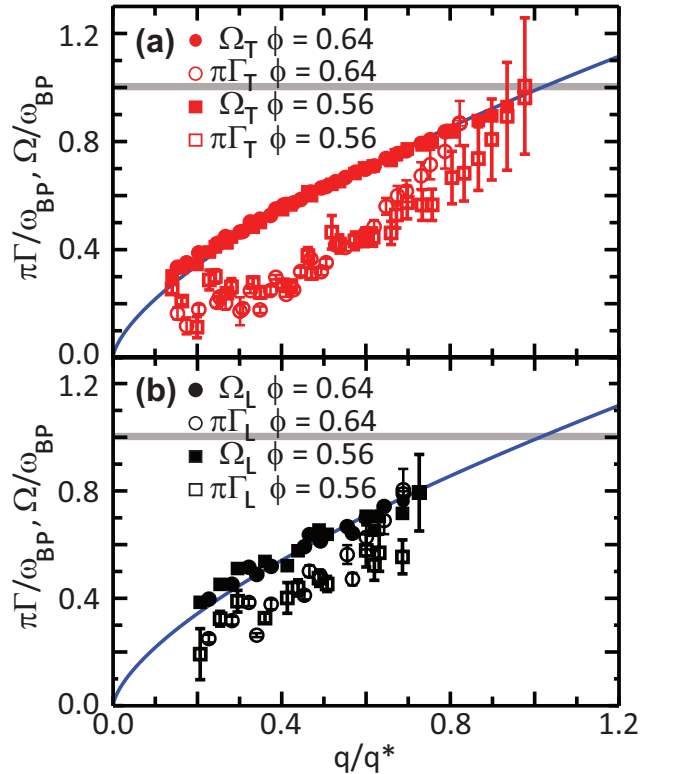

FIG. 5: (Color online)(a) $\Omega(q)$ and $\pi\Gamma(q)$ scaled by the BP frequency, ω_{BP} as determined from Fig. 3, for transverse modes for both $\phi = 0.56$ and $\phi = 0.64$. q^* is chosen such that $\Omega(q^*)/\omega_{BP} = 1$. (b) Same as (a) but for longitudinal modes. Solid lines are $q^{2/3}$ (see text). The $\Omega(q)$ curves collapse almost perfectly to the $q^{2/3}$ form at both densities on both branches, while the $\pi\Gamma(q)$ curves show slightly more scatter. The horizontal gray line is ω_{BP}.

tions in elastic properties. This is not at all what we observe. The Debye scaling is rather special and fails in most structural glasses [1, 2], even when they are far from any transition. Other systems near a transition, such as

colloidal glasses near the jamming transition, do exhibit pronounced changes in mode structure indicating a lack of scaling [4]. This makes the invariance in our system all the more striking.

IV. CONCLUSIONS

In conclusion, we have measured the DSF and DOS in a disordered colloidal crystal. Both transverse and longitudinal branches of the DSF are invariant under changes in ϕ when rescaled by the Debye level, even near the melt-

ing transition. Both branches become overdamped (the IR limit) at a common frequency, somewhat below the BP frequency. This shows that while disordered crystals exhibit some common features with structural glasses, many vibrational properties depend on the detailed nature of the underlying disorder.

[1] K. Niss, B. Begen, B. Frick, J. Ollivier, A. Beraud, A. Sokolov, V. N. Novikov, and C. Alba-Simionesco, Phys. Rev. Lett. **99**, 055502 (2007).
[2] B. Rufflé, S. Ayrinhac, E. Courtens, R. Vacher, M. Foret, A. Wischnewski, and U. Buchenau, Phys. Rev. Lett. **104**, 067402 (2010).
[3] A. Monaco, A. I. Chumakov, G. Monaco, W. A. Crichton, A. Meyer, L. Comez, D. Fioretto, J. Korecki, and R. Rüffer, Phys. Rev. Lett. **97**, 135501 (2006).
[4] K. Chen, W. G. Ellenbroek, Z. Zhang, D. T. N. Chen, P. Yunker, S. Henkes, C. Brito, O. Dauchot, W. van Saarloos, A. J. Liu, et al., Phys. Rev. Lett. **105**, 025501 (2010).
[5] W. K. Kegel and A. van Blaaderen, Science **287**, 290 (2000).
[6] D. G. A. L. Aarts, M. Schmidt, and H. N. W. Lekkerkerker, Science **304**, 847 (2004).
[7] U. Gasser, E. R. Weeks, A. Schofield, P. N. Pusey, and D. A. Weitz, Science **292**, 258 (2001).
[8] A. M. Alsayed, M. F. Islam, J. Zhang, P. J. Collings, and A. G. Yodh, Science **309**, 1207 (2005).
[9] E. R. Weeks, J. C. Crocker, A. C. Levitt, A. Schofield, and D. A. Weitz, Science **287**, 627 (2000).
[10] J. Mattsson, H. M. Wyss, A. Fernandez-Nieves, K. Miyazaki, Z. Hu, D. R. Reichman, and D. A. Weitz, Nature **462**, 83 (2009).
[11] D. Kaya, N. L. Green, C. E. Maloney, and M. F. Islam, Science **329**, 656 (2010).
[12] W. Schirmacher, G. Diezemann, and C. Ganter, Phys. Rev. Lett. **81**, 136 (1998).
[13] S. N. Taraskin, Y. L. Loh, G. Natarajan, and S. R. Elliott, Phys. Rev. Lett. **86**, 1255 (2001).
[14] A. Ghosh, V. K. Chikkadi, P. Schall, J. Kurchan, and D. Bonn, Phys. Rev. Lett. **104**, 248305 (2010).
[15] Y. Han, Y. Shokef, A. M. Alsayed, P. Yunker, T. C. Lubensky, and A. G. Yodh, Nature **456**, 898 (2008).
[16] J. C. Crocker and D. G. Grier, J. Colloid Interface Sci. **179**, 298 (1996).
[17] J. C. Crocker and B. D. Hoffman, Methods Cell Biol. **83**, 141 (2007).
[18] H. Shintani and H. Tanaka, Nature Mater. **7**, 870 (2008).
[19] H. R. Schober, J. of Phys: Condens. Matter **16**, S2659 (2004).
[20] J. Horbach, W. Kob, and K. Binder, Eur. Phys. J. B **19**, 531 (2001).
[21] P. M. Chaikin and T. C. Lubensky, *Principles of Condensed Matter Physics* (Cambridge University Press, 2000).
[22] G. Ruocco and F. Sette, Journal of Physics: Condensed Matter **13**, 9141 (2001).
[23] G. Monaco and V. M. Giordano, PNAS **106**, 3659 (2009).
[24] J. Horbach, W. Kob, and K. Binder, Journal of Non-Crystalline Solids **235-237**, 320 (1998).
[25] S. N. Taraskin and S. R. Elliott, Journal of Physics: Condensed Matter **11**, A219 (1999).
[26] L. Angelani, M. Montagna, G. Ruocco, and G. Viliani, Phys. Rev. Lett. **84**, 4874 (2000).
[27] G. Monaco and S. Mossa, PNAS **106**, 16907 (2009).
[28] T. Scopigno, J.-B. Suck, R. Angelini, F. Albergamo, and G. Ruocco, Phys. Rev. Lett. **96**, 135501 (2006).
[29] B. Rufflé, G. Guimbretière, E. Courtens, R. Vacher, and G. Monaco, Phys. Rev. Lett. **96**, 045502 (2006).